View Article Online
DOI: 10.1039/D0CY01751E

ARTICLE

Direct Design of Active Catalysts for Low Temperature Oxidative Coupling of Methane via Machine Learning and Data Mining

Received 00th January 20xx,
Accepted 00th January 20xx

DOI: 10.1039/x0xx00000x

Junya Ohyama,*[a] Takaaki Kinoshita,[b] Eri Funada,[b] Hiroshi Yoshida,[a] Masato Machida,[a] Shun Nishimura,[c] Takeaki Uno,[d] Jun Fujima,[e] Itsuki Miyazato,[e] Lauren Takahashi[e] and Keisuke Takahashi*[e]

Direct design of low temperature oxidative coupling of methane (OCM) catalysts is proposed via machine learning and data mining. 58 OCM catalysts are experimentally synthesized and evaluated. Collected 58 data are then classified by unsupervised machine learning in multi-dimensional space where active catalysts group for low temperature OCM is identified. Data mining then identifies the physical rule within the group. Catalysts satisfying such physical rule is designed where 2 undiscovered low temperature OCM catalysts are found and experimentally validated. Thus, machine learning and data mining reveal the hidden physical rule behind the catalysis leading to the direct design of catalysts. Hence, machine learning and data mining open up the insight of powerful strategy for designing catalysts.

Introduction

Direct design of solid catalysts has been a challenging matter as catalytic activity is strongly coupled with experimental conditions and how the elements of the periodic table are combined.[1, 2] In general, numerous experiments are performed in order to better characterize how the elements affect various catalytic properties. By better understanding how the elements affect catalysis and the roles they play in solid catalysts, steps can be taken closer towards effective catalyst design. Additionally, by understanding the underlying physical and chemical patterns and rules that are hidden within catalyst data, one can then, in principle, design catalysts more directly by using said trends and patterns.[3-5] In such circumstances, data science plays a crucial role in revealing patterns hidden within catalyst data where various factors affecting catalytic activities are simultaneously treated within a multi-dimensional space.[5-8] In particular, unsupervised machine learning and frequent item-set mining (FIM) within the data mining are of interest. Unsupervised machine learning is a type of machine learning used for identifying hidden patterns and groups within datasets where Gaussian Mixture Model (GMM) is implemented[9, 10]. Data mining is applied to find all significant combinations of physics and chemistry in the data. [9, 10] Such data science can provide potential catalyst candidates from a large space of catalyst components. It should be noted that the prediction by the data science does not guarantee targeted performance for each catalyst component, but rather, it provides a list of possible components which might include new catalysts. Here, the direct design of catalysts from a large space of catalyst components is proposed through combinatorial use of unsupervised machine learning and data mining.

OCM is chosen as a prototype reaction where the reaction aims the direct conversion of methane (CH_4) into ethylene/ethane (C_2H_4/C_2H_6, C2 compounds). OCM is one of the promising methods offering energy-efficient conversion of methane to C2 compounds as platform chemicals.[11-14] Previous studies have shown that alkali and alkaline earth metals are effective elements for OCM catalysts.[12, 15, 16] Among them, Na catalysts modified with Mn and W, namely, Mn-Na_2WO_4/SiO_2, have been developed and studied as catalysts showing relatively high performance for OCM; however, their C2 selectivity and yield do not meet the practical interest.[11, 17-21] This might be due to the high reaction temperature, e.g., more than 700 °C, where non-selective radical reactions in gas phase proceed.[11] In addition, such high reaction temperature requires special materials for the reactors with heat durability. Thus, OCM catalysts activating CH_4 at lower temperature are desirable. In previous studies, catalyst materials containing rare earth elements such as La and Ce are effective for low-temperature C-H activation of hydrocarbons and OCM reaction.[22-25] For instance, La_2O_3-CeO_2 nanofiber has been developed as an OCM catalyst exhibiting relatively high C2 selectivity at low temperature.[26, 27] Here, active catalysts for low temperature OCM are explored using unsupervised machine learning and FIM.

[a] Faculty of Advanced Science and Technology, Kumamoto University, 2-39-1 Kurokami, Chuo-ku, Kumamoto, 860-8555 Japan. E-mail: ohyama@kumamoto-u.ac.jp (J.O.)
[b] Graduate School of Science and Technology, Kumamoto University, 2-39-1 Kurokami, Chuo-ku, Kumamoto, 860-8555, Japan.
[c] Graduate School of Advanced Science and Technology, Japan Advanced Institute of Science and Technology (JAIST), 1-1 Asahidai, Nomi, 923-1292 Japan.
[d] National Institute of Informatics (NII), 2-1-2 Hitotsubashi, Chiyoda-ku, 101-8430 Japan.
[e] Department of Chemistry, Hokkaido University, N-15 W-8, Sapporo 060-0815, Japan. E-mail: keisuke.takahashi@eng.hokudai.ac.jp (K.T.)

† Electronic Supplementary Information (ESI) available: reaction results. See DOI: 10.1039/x0xx00000x

View Article Online
DOI: 10.1039/D0CY01751E

Workflow

Direct design of active catalysts for low temperature OCM is carried out following five main steps. The details of the workflow followed are illustrated in Figure 1. The first step is data collection. Here, data is procured via experiment where 58 OCM catalysts are experimentally prepared and evaluated. The data collected from the 58 OCM catalysts are then classified based on C2 yield at 400, 500, 600, 700, 800, and 900°C where GMM within the unsupervised machine learning is implemented. Within the classified groups, active catalyst groups for low temperature OCM are identified. Data mining is then implemented in order to determine common physical rules within the groups. Once the physical rules of active catalysts for low temperature OCM are identified, catalysts are then designed based on the physical rules that are deemed to result in low temperature OCM. Lastly, experimental synthesis and validation are performed.

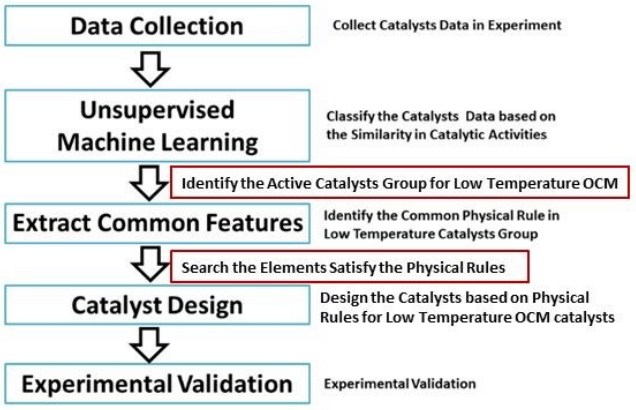

Figure 1. The roadmap for design low temperature OCM catalysts.

Results and Discussion

Experimental Method and Data Collection

OCM data collection for machine learning and data mining are performed in experiment. In particular, 58 catalysts shown in Figure 2 are synthesized and evaluated where 58 catalysts consist of various mono-metal oxides, 1wt% M/La_2O_3, and 1 wt% indium (In) modified rare earth oxide, 0.5-0.01wt% In/La_2O_3, 0.1wt% In/Nd_2O_3, and 0.1wt% In/Eu_2O_3 (Table S1-3). OCM reaction is conducted by flowing a 72% CH_4/ 22% O_2/ 6% N_2 gas (34 mL min^{-1}) to a catalyst (50 mg) at 400 to 900 °C in a fixed bed flow reactor. Figure 2(a) shows the reaction results over 19 mono-metal oxides at 500, 600, and 700 °C. The details of all reaction data are presented in the Supplementary Information. Three rare-earth metal oxides provide C2 compounds from 500 °C: , Nd_2O_3, Eu_2O_3, and Pr_6O_{11} exhibit C2 yield of 14, 13, and 3%, respectively at the low temperature of 500°C. On the other hand, the other oxides, in particular, typical elements need more than 600°C for significant C2 production. In addition, $Mn\text{-}Na_2WO_4/SiO_2$, a reference catalyst, produces C2 compounds at more than 800°C (Table S1), though it exhibits a significant C2 yield higher than 12%. Thus, rare-earth metal oxides are effective for the low-temperature OCM, which agrees with the results in the literature.[24, 26, 27]

Surface modification of La_2O_3 with a different metal species is performed using 25 elements for further exploration of catalyst materials for the low temperature OCM as shown in Figure 2(b). Figure 2(b) shows the reaction results over the modified La_2O_3 with 1wt% metal loading (1wt% M/La_2O_3). Alkaline and alkaline earth metals modified La_2O_3 catalysts exhibit superior low-temperature activity compared to La_2O_3, agreeing with the previous results in the literature.[28, 29] For instance, Mg/, Ca/, Sr/ and Ba/La_2O_3 provide C2 yield of 8%, 17%, 17%, and 10% at 500°C. In addition, 1wt% In/La_2O_3 (C2 yield 14%), Zn/La_2O_3 (15%), Fe/La_2O_3 (11%), and Ag/La_2O_3 (9%) also effective for the low-temperature OCM. Therefore, the surface modification with basic and transition metals can also increase the low temperature OCM activity. The In loading is varied in In/La_2O_3 from 0.01 to 1 wt%, and the other rare-earth metal oxides are also modified with the same In loadings. As shown in Figure 2(c), the catalytic performance of In/La_2O_3 depends on the In loading, and shows the highest at 0.1 wt%. The low-temperature activity of La_2O_3, Sm_2O_3, and Gd_2O_3 are improved by In modifications. In contrast, in the case of Nd_2O_3 and Eu_2O_3, the catalytic performance is not improved or decreased. Thus, the effect of surface modifications with another metal depends on the loading and the kind of metal oxides, possibly due to variation of OCM-effective surface sites such as surface oxygen species or basicity.[24, 30] Thus, various 58 OCM catalysts are experimentally performed and collected as data.

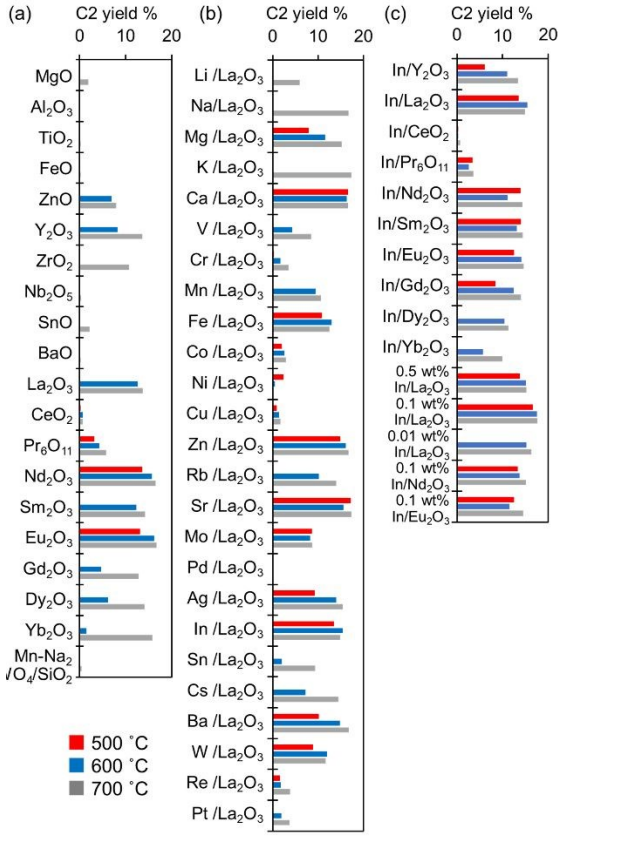

Figure 2. C2 yield during the OCM reaction at 500°C (red), 600°C (blue), and 700°C (gray) over (a) various mono-metal oxides and Mn-Na_2WO_4/SiO_2 as a reference; (b) 1wt% M/La_2O_3; (c) 1 wt% In modified rare earth oxide, 0.5-0.01wt% In/La_2O_3, 0.1wt% In/Nd_2O_3, and 0.1wt% In/Eu_2O_3.

Machine Learning

Machine learning is performed with the collected 58 catalysts data. In particular, unsupervised machine learning is implemented in order to classify the OCM catalysts based on how catalysts response against the change of temperature. Here, GMM within scikit-learn, unsupervised machine learning, is used where the number of component and covariance are set to 5 and full, respectively.[31] The convergence threshold is set to 1e-3. The following 6 descriptors are selected for GMM: C2 yield at 400, 500, 600, 700, 800, and 900°C for each catalyst. Classified catalysts by GMM are illustrated in Figure 3. Unique feature of each group is then investigated via parallel coordinate as shown in Figure 4 where parallel coordinate represents the C2 yield at 400, 500, 600, 700, 800, and 900°C. Color in Figure 4 represents the predicted group by GMM. Figure 4 demonstrates that GMM classifies the catalysts based on change of C2 yield against the temperature. More precisely, catalysts in group 1 are less active catalysts. Catalysts in group 0 and 3 have production of C2 at above 600°C and 700°C, respectively. Catalysts in group 4 have production of C2 at 500°C; however, the amount of C2 yield is less than one in group 2. In such circumstance, catalysts in group 2 can be considered to be active catalysts at low temperature as large production of C2 yield is observed at 500°C. One can consider that low temperature OCM catalysts can be designed in principle if common physical rules in group 2 are revealed. Thus, GMM can classify catalysts data based on the catalysts' unique features in a rational manner.

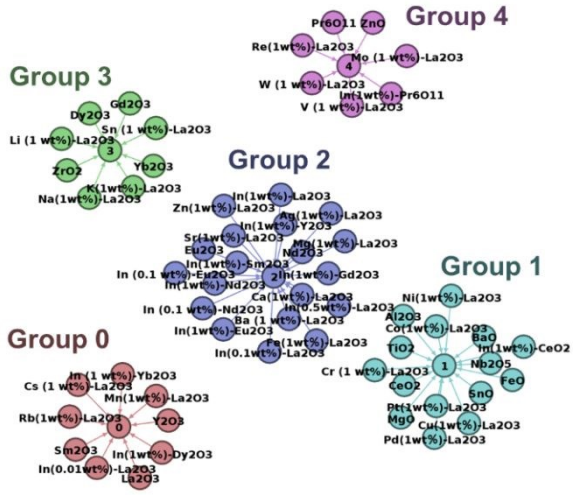

Figure 3. Classified OCM catalysts by GMM.

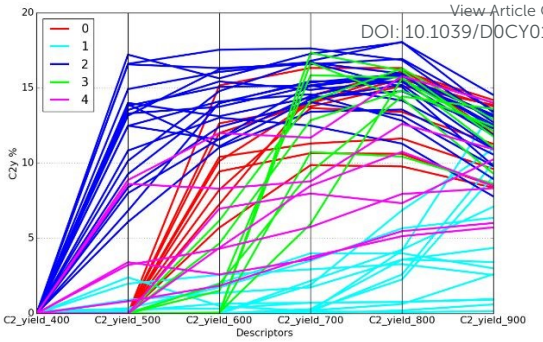

Figure 4. Parallel coordinate of C2 yield at 400, 500, 600, 700, 800, and 900°C. Color represents the predicted group by GMM.

Extracting Common Physical Features

In order to search for the common physical rules of Group 2 shown in Figure 3, an itemset mining analysis is conducted for physical properties of each catalyst. The explanation of itemset mining is described in the Method section. Focusing on elements in the main metal oxides (MOx) and modifiers (Ad), various elemental property values are collected from a periodic table.[32] All value ranges for MOx and Ad are presented in Table 1. Each quantity is discretized and itemized in the following manner for the use of itemset mining. First, items (or categories) representing inequality expressions are determined for each property by dividing the range of values of each given property value of the 58 catalysts by a given division number. The resulting number is then used to establish the range for each item. For example, if the division number is four, then six items are able to be created. When applying this to periodic table groups (which are 14 in total), then the resulting value "3.5" is used to determine the boundaries between items. Given this, a division number of 4 is used and the periodic table groups (Group) of Ad are divided into six items: "Ad_Group < 3.5", "3.5 ≦ Ad_Group", "Ad_Group < 7.0", "7.0 ≦ Ad_Group", "Ad_Group < 10.5", and "10.5 ≦ Ad_Group". As an example, the record corresponding to Fe, which belongs to periodic group 8, has three items for "Ad_Group", such that "3.5 ≦ Ad_Group", "7.0 ≦ Ad_Group", and "Ad_Group < 10.5". In this way, the 19 catalysts in Group 2 are converted to records that have items generated in the above way for all properties listed in Table 1. In this study, 20 is used as the division number in order to narrow down rules for searching catalysts. Subsequently, a part of functionality of Linear time closed itemset miner (LCM)[9] is used to find the common items for all catalysts in Group 2 where the details of how LCM is applied are discussed in the Method section. LCM found a common itemset included in all records corresponding to the 19 catalysts in Group 2. Finally, the common items for all properties are consolidated to represent common ranges as shown in Table 2. These ranges specify the common rules which must be satisfied by the elements of the catalysts in Group 2. From here, the elements in the same range as M of MOx and Ad in Group 2 are investigated and listed in Table 3. Note that the list in Table 3 includes the elements not found in the experimental data: e.g., Al, Sc, Ga, Sr, and Cd for Ad. More importantly, the

combinations of MOx and Ad in Table 3 can form new catalyst compositions that are not only not present in the original data used in this study but also not present in previous literature. In other words, new catalyst materials are able to be predicted using the data mining method.

In order to validate the prediction by the itemset mining method, new Ad/MOx catalysts are prepared by choosing Y_2O_3 as MOx and Al, Ca, Ni, Zn, and Ag as Ad on the basis of Table 3. The OCM reaction results using the predicted catalysts are presented in Figure 5, where Al/Y_2O_3 and Ag/Y_2O_3 exhibit C2 yield at the low temperature of 500°C, where the other catalysts do not show activity at 500°C (Table S4). Note that Y_2O_3 alone does not produce C2 at 500°C as shown in Figure 2. To our knowledge, the compositions of Al/Y_2O_3 and Ag/Y_2O_3 have not been previously reported as the OCM catalysts in the literature.[11, 12] Thus, new catalyst materials are developed by the machine learning and the itemset mining method. The results indicate that the approach taken in this work could innovate how catalyst materials are designed and developed.

A possible chemical reason for the low temperature OCM activity of the Group 2 catalysts and the predicted catalysts are investigated. According to the literature, the surface oxygen species on OCM catalysts, more specifically, the ratio of the surface superoxide (O_2^-) to the lattice oxygen (O^{2-}), can describe the low temperature activity.[24] Thus, the surface oxygen species of several catalysts including the Group 0-4 catalysts and the predicted catalysts was analyzed by X-ray photoelectron spectroscopy (XPS) as shown in Figure S1. Peak fitting analysis suggested that the O1s XPS of the catalysts are composed of three peaks at 529-530, 531-532, and 533-534 eV, which are assignable to O_2^-, carbonate (CO_3^{2-}), and O^{2-}, respectively.[24] Figure S2 shows a plot of the C2 yield at 500 °C against the ratio of O1s XPS peak areas at 529-530 and 533-534 eV of the catalysts. There is a tendency that C2 yield increases with an increase of the ratio and then decreased, although the catalysts containing alkaline and alkaline earth metals are out of the trend. Thus, one can consider that the common catalyst features extracted by the data science techniques contain descriptors of catalytically active surface oxygen species and other activity controlling factors, and thus give a list of possible candidates containing Al/Y_2O_3 and Ag/Y_2O_3 which actually show the low temperature activity.

Table 1. Various elemental properties and their value ranges of MOx and Ad.

Elemental property	MOx	Ad
Abundance in crust (Abundance) (mg/kg)	2 - 82300	0 - 56300
Allen electronegativity (Allen_e-neg)	0 - 1.824	0 - 1.88
Atomic radius (Å)	1.18 - 2.53	0 - 2.98
Atomic weight	24.3059 - 173.045	0 - 195.08-
Boiling point (K)	1180 - 5017	0 - 5869
Covalent radius (Å)	0 - 1.98	0 - 2.25
Crystal radius (Å)	0.53 - 1.49	0 - 1.81
Density (g/cm^3)	1.738 - 8.57	0 - 21.46
Electron configuration [a]	1 - 2	0 - 3
Group [b]	2- 14	0 - 14
Heat capacity (J/gK)	0.155 - 1.023	0 - 3.582
Ionic radius (Å)	1.25 - 2.15	0 - 2.6
Melting point (K)	505.08 - 2750	0 - 3695
Pauling electronegativity (Pauling_e-neg)	0 - 1.96	0 - 2.36
Period [b]	3 - 6	0 - 6
Thermal conductivity	0.1 - 2.3	0 - 4.2
Valence electron	1 - 2	0 - 10
Van_der_Waals_radius (Å)	0 - 2.17	0 - 2.75
Electron affinity (e-aff-ev) (eV)	0 - 1.11207	-1 - 2.1251
Electron affinity (e-aff-kJmol) (kJ/mol)	0 - 107.2984	0 - 205.041
1st Ionization energy (ion-e_1st) (kJ/mol)	502.9 - 906.4	0 - 906.4
2nd Ionization energy (ion-e_2nd) (kJ/mol)	965.2 - 1816.7	0 - 7298.1
3rd Ionization energy (ion-e_3rd) (kJ/mol)	1850.3 - 7732.7	0 - 11815
4rd Ionization energy (ion-e_4th) (kJ/mol)	0 - 11577	0 - 10542.5
5rd Ionization energy (ion-e_5th) (kJ/mol)	0 - 14842	0 - 13630
6rd Ionization energy (ion-e_6th) (kJ/mol)	0 - 18379	0 - 18020
7rd Ionization energy (ion-e_7th) (kJ/mol)	0 - 23326	0 - 21711
8rd Ionization energy (ion-e_8th) (kJ/mol)	0 - 27465	0 - 25661
9rd Ionization energy (ion-e_9th) (kJ/mol)	0 - 31853	0 - 31653
10rd Ionization energy (ion-e_10th) (kJ/mol)	0 - 38473	0 - 141362

[a] Number indicating electron number N_e in the outermost sphere. 1: $N_e < 2$, 2: $2 \le N_e < 10$, 3: $10 \le N_e$. [b] On the periodic table.

Conclusions

Direct design of low temperature OCM is proposed via machine learning and data mining. 58 OCM catalysts data are prepared and evaluated in experiments. Unsupervised machine learning classified the 58 OCM catalysts based on response of C2 yield against temperature changes. Unsupervised machine learning reveals the catalysts group which is active at low temperature OCM. Data mining identified the common physical rules in the active group. Low temperature OCM catalysts are then designed based on satisfying the physical rules. In particular, predicted Al/Y_2O_3 and Ag/Y_2O_3 are discovered to be active at low temperature OCM in experiment. Thus, the proposed direct design of catalysts discovered the two unreported active OCM catalysts at low temperature. Thus, machine learning and data mining would innovate how catalysts are searched and gives a strategy for designing catalysts.

View Article Online
DOI: 10.1039/D0CY01751E

Table 2. The common property value ranges in MOx and Ad of the group 2.

MOx	Ad
MOx_Abundance < 4116.9	Ad_Atomic_radius < 2.533
MOx_Allen_e-neg < 1.1856	Ad_Atomic_weight < 146.31300000000002
MOx_Atomic_radius < 2.3949999999999996	Ad_Boiling_point < 3227.95
MOx_Atomic_radius ≥ 1.9224999999999999	Ad_Covalent_radius < 2.025
MOx_Atomic_weight < 158.17109	Ad_Crystal_radius < 1.5385
MOx_Atomic_weight ≥ 83.80153999999999	Ad_Density < 10.73
MOx_Boiling_point < 3865.9	Ad_Electron_configulation < 2.1
MOx_Boiling_point ≥ 1755.55	Ad_Group < 13.299999999999999
MOx_Covalent_radius < 1.782	Ad_Heat_capacity < 1.0745999999999998
MOx_Crystal_radius < 1.3940000000000001	Ad_Ionic_radius < 2.21
MOx_Crystal_radius ≥ 1.01	Ad_Melting_point < 1847.5
MOx_Density < 8.2284	Ad_Pauling_e-neg < 2.006
MOx_Density ≥ 4.1292	Ad_Valence_electron < 2.5
MOx_Electron_configulation < 1.05	Ad_Van_der_Waals_radius < 2.0625
MOx_Group < 3.2	Ad_e-aff-ev < 1.3438250000000003
MOx_Group ≥ 2.6	Ad_e-aff-ev ≥ -0.062470000000000026
MOx_Heat_capacity < 0.3286	Ad_e-aff-kJmol < 133.27665000000002
MOx_Ionic_radius < 1.97	Ad_ion-e_10th < 42408.600000000006
MOx_Ionic_radius ≥ 1.79	Ad_ion-e_2nd < 2189.4300000000003
MOx_Melting_point < 1852.0320000000002	Ad_ion-e_3rd < 8270.5
MOx_Melting_point ≥ 1066.31	
MOx_Pauling_e-neg < 1.274	
MOx_Period ≥ 4.95	
MOx_Thermal_conductivity < 0.21	
MOx_Valence_electron ≥ 1.9500000000000002	
MOx_Van_der_Waals_radius < 0.1085	
MOx_e-aff-ev < 0.556035	
MOx_e-aff-ev ≥ 0.11120699999999999	
MOx_e-aff-kJmol < 53.64919999999999	
MOx_ion-e_10th < 19236.5	
MOx_ion-e_1st < 603.775	
MOx_ion-e_1st ≥ 523.0749999999999	
MOx_ion-e_2nd < 1220.65	
MOx_ion-e_2nd ≥ 1007.7750000000001	
MOx_ion-e_3rd < 2438.54	
MOx_ion-e_4th < 6367.35	
MOx_ion-e_4th ≥ 3473.1000000000004	
MOx_ion-e_5th < 8163.1	
MOx_ion-e_6th < 9189.5	
MOx_ion-e_7th < 11663.0	
MOx_ion-e_8th < 13732.5	
MOx_ion-e_9th < 14333.85	

Table 3. The elements having the same items as MOx and Ad of the group 2 catalysts.

MOx	Ad
Y, La, Nd Sm, Eu, Gd	Mg, Al, Ca, Sc, Fe, Co, Ni, Cu, Zn, Ga, Sr, Ag, Cd, In, Ba, Es, Fm, Md, No, Lr, Rf, Db, Sg, Bh, Hs, Mt, Ds, Rg, Cn

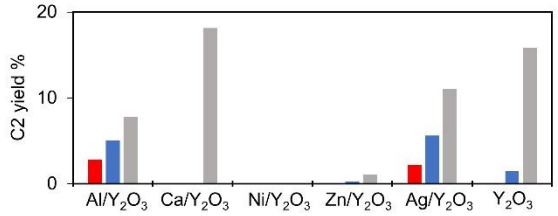

Figure 5. C2 yield during the OCM reaction at 500°C (red), 600°C (blue), and 700°C (gray) over the predicted catalysts together with that over Y_2O_3 for comparison.

Methods

Catalyst preparation

The metal oxides and the precursors for modifiers are commercially available as listed in Table S5. The modified metal oxides are prepared by a conventional impregnation method where metal oxide powder is impregnated with aqueous solution of metal precursor. After the impregnation, the powder is dried at 110 °C and then calcined at 600 °C to prepare the modified metal oxides. Mn-Na_2WO_4/SiO_2 is prepared by impregnation of SiO_2 in an aqueous solution containing $Mn(NO_3)_2$ and Na_2WO_4. The suspension is stirred at 50 °C for 24 h, and then evaporated at 65 °C. The resulting solid is dried at 110 °C overnight and calcined at 1000 °C for 3 h to obtain Mn-Na_2WO_4/SiO_2 having 1.9wt% Mn and 5.0wt% Na_2WO_4

Catalytic reaction

OCM is performed on a conventional fixed bed reactor, where catalyst powder of 50 mg is put in a quartz tube with inside diameter of 4 mm. The catalyst is pretreated under O_2 flow of 8.3 mL min^{-1} at 400 °C. OCM reaction is conducted at 400-900 °C under a mixed gas of 24 mL min^{-1} CH_4, 7.5 mL min^{-1} O_2, and 2 mL min^{-1} N_2. The effluent gas is analyzed by gas chromatograph with a thermal conductivity detector (Agilent 490). C2 yield is determined by ((effluent C_2 conc. / effluent N_2 conc.) / (initial CH_4 conc. / initial N_2 conc.)) ×2×100 (%).

Linear Time Closed Itemset Miner (LCM)

LCM within itemset mining is implemented in order to see the common rule in catalysts.[9] Within LCM, itemset mining inputs a transaction database and output all frequent itemsets in the database. A transaction database is composed of records such that each record is a set of items. Here items are some entities, for example {banana, apple, orange, grape} that are three items. An itemset is a set of items such as {banana, orange}. An example of a transaction database is {banana, orange}, {banana, apple, grape}, and {apple, orange, grape}. The frequency of an itemset is defined by the number of records including the itemset. For example, the frequency of {apple, grape} in the above example database is two, since it is included in the

second and the third records. For given a user specified support threshold θ, an itemset is called frequent itemset if its frequency is no less than θ. Itemset mining algorithm inputs a transaction database and the user specified support threshold, and outputs all the frequent itemsets in the database. Note that in general, a transaction database may have numerous frequent itemsets, and an itemset mining algorithm always outputs all frequent itemsets. Thus, any two different itemset mining tools always produce the same solution, thus the difference on their computational time. Hence, LCM is chosen due to its computational speeds.

Characterization

XPS measurement is performed with a K-ALPHA instrument (Thermo Fisher Scientific, UK) using Al *Kα* radiation. The energy is calibrated by referencing the C1s peak to 285.0 eV.

Conflicts of interest

There are no conflicts to declare.

Acknowledgements

This work is funded in part by the Japan Science and Technology Agency (JST) CREST (JPMJCR17P2), and JSPS KAKENHI Grant-in-Aid for Young Scientists (B) Grant NumberJP17K14803.

Contributions

J.O., T.K. and E.F. conducted the catalyst preparation and the reaction evaluation. H.Y., M.M. and S.N. participated in the experiments. T.U. developed LCM. J.F. and I.M. performed the item set mining. I.M., L.T. and K.T. performed the machine learning and the itemset mining. J.O. and K.T. mainly wrote the paper. All authors contributed to the design of study, discussed the results, and reviewed the manuscript.

References

1 J. M. Thomas, W. J. Thomas and H. W. Salzberg, *J. Electrochem. Soc.*, 1967, **114**, 279C.
2 F. Zaera, *Catal. Lett.*, 2012, **142**, 501-516.
3 A. J. Medford, M. R. Kunz, S. M. Ewing, T. Borders and R. Fushimi, *ACS Catal.*, 2018, **8**, 7403-7429.
4 J. K. Nørskov and T. Bligaard, *Angew. Chem. Int. Ed.*, 2013, **52**, 776-777.
5 K. Takahashi, L. Takahashi, I. Miyazato, J. Fujima, Y. Tanaka, T. Uno, H. Satoh, K. Ohno, M. Nishida, K. Hirai, J. Ohyama, T. N. Nguyen, S. Nishimura and T. Taniike, *ChemCatChem*, 2019, **11**, 1146-1152.
6 J. R. Kitchin, *Nat. Catal.*, 2018, **1**, 230-232.
7 H. Kulik, *Abstracts of Papers of the American Chemical Society*, 2018, **255**.
8 P. Schlexer Lamoureux, K. T. Winther, J. A. Garrido Torres, V. Streibel, M. Zhao, M. Bajdich, F. Abild-Pedersen and T. Bligaard, *ChemCatChem*, 2019, **11**, 3581-3601.
9 T. Uno, M. Kiyomi and H. Arimura, presented in part at the Proceedings of the 1st international workshop on open source data mining: frequent pattern mining implementations, Chicago, Illinois, 2005.
10 S. Naulaerts, P. Meysman, W. Bittremieux, T. N. Vu, W. Vanden Berghe, B. Goethals and K. Laukens, *Brief Bioinform.*, 2015, **16**, 216-231.
11 E. V. Kondratenko, T. Peppel, D. Seeburg, V. A. Kondratenko, N. Kalevaru, A. Martin and S. Wohlrab, *Catal. Sci. Tech.*, 2017, **7**, 366-381.
12 U. Zavyalova, M. Holena, R. Schlögl and M. Baerns, *ChemCatChem*, 2011, **3**, 1935-1947.
13 R. Schmack, A. Friedrich, E. V. Kondratenko, J. Polte, A. Werwatz and R. Kraehnert, *Nat. Commun.*, 2019, **10**, 441.
14 K. Suzuki, T. Toyao, Z. Maeno, S. Takakusagi, K.-i. Shimizu and I. Takigawa, *ChemCatChem*, 2019, **11**, 4537-4547.
15 K. Takahashi, I. Miyazato, S. Nishimura and J. Ohyama, *ChemCatChem*, 2018, **10**, 3223-3228.
16 T. N. Nguyen, T. T. P. Nhat, K. Takimoto, A. Thakur, S. Nishimura, J. Ohyama, I. Miyazato, L. Takahashi, J. Fujima, K. Takahashi and T. Taniike, *ACS Catal.*, 2020, **10**, 921-932.
17 S. Arndt, T. Otremba, U. Simon, M. Yildiz, H. Schubert and R. Schomäcker, *Appl. Catal. A*, 2012, **425-426**, 53-61.
18 S. Pak, P. Qiu and J. H. Lunsford, *J. Catal.*, 1998, **179**, 222-230.
19 U. Simon, O. Görke, A. Berthold, S. Arndt, R. Schomäcker and H. Schubert, *Chem. Eng. J.*, 2011, **168**, 1352-1359.
20 J. Ohyama, S. Nishimura and K. Takahashi, *ChemCatChem*, 2019, **11**, 4307-4313.
21 I. Miyazato, S. Nishimura, L. Takahashi, J. Ohyama and K. Takahashi, *J. Phys. Chem. Lett.*, 2020, **11**, 787-795.
22 D. J. Wang, M. P. Rosynek and J. H. Lunsford, *J. Catal.*, 1995, **155**, 390-402.
23 Y. Zhang, J. Xu, X. Xu, R. Xi, Y. Liu, X. Fang and X. Wang, *Catal. Today*, 2019, DOI: https://doi.org/10.1016/j.cattod.2019.06.060.
24 J. Xu, Y. Zhang, X. Xu, X. Fang, R. Xi, Y. Liu, R. Zheng and X. Wang, *ACS Catal.*, 2019, **9**, 4030-4045.
25 A. Sato, S. Ogo, K. Kamata, Y. Takeno, T. Yabe, T. Yamamoto, S. Matsumura, M. Hara and Y. Sekine, *Chem. Commun.*, 2019, **55**, 4019-4022.
26 D. Noon, B. Zohour and S. Senkan, *J. Nat. Gas Sci. Eng.*, 2014, **18**, 406-411.
27 D. Noon, A. Seubsai and S. Senkan, *ChemCatChem*, 2013, **5**, 146-149.
28 V. J. Ferreira, P. Tavares, J. L. Figueiredo and J. L. Faria, *Ind. Eng. Chem. Res*, 2012, **51**, 10535-10541.
29 J. Song, Y. Sun, R. Ba, S. Huang, Y. Zhao, J. Zhang, Y. Sun and Y. Zhu, *Nanoscale*, 2015, **7**, 2260-2264.
30 P. Schwach, X. Pan and X. Bao, *Chem. Rev.*, 2017, **117**, 8497-8520.
31 F. Pedregosa, G. Varoquaux, A. Gramfort, V. Michel, B. Thirion, O. Grisel, M. Blondel, P. Prettenhofer, R. Weiss, V. Dubourg, J. Vanderplas, A. Passos, D. Cournapeau, M. Brucher, M. Perrot and E. Duchesnay, *J. Mach. Learn. Res.*, 2011, **12**, 2825-2830.
32 T. Gray, M. Whitby and N. Mann, The photographic periodic table of the elements, https://periodictable.com/index.html).